

## Article

# Isothermal Oxidation TGO Growth Behaviors of Laser-Remolten LZO/YSZ Thermal Barrier Coatings

Wensheng Li <sup>1,2,\*</sup>, Ziyu Li <sup>2</sup>, Guosheng An <sup>2,\*</sup>, Bo Cheng <sup>2</sup>, Qiang Song <sup>1</sup>, Jinqun Sun <sup>1</sup>, Victor Vaganov <sup>3</sup>, Canming Wang <sup>1</sup> and Georg Goransky <sup>3</sup>

<sup>1</sup> School of Materials Science and Engineering, Shandong University of Science and Technology, Qingdao 266590, China; songq2008@sdust.edu.cn (Q.S.); nanomaterial@163.com (J.S.); wangcanming@sdust.edu.cn (C.W.)

<sup>2</sup> State Key Laboratory of Advanced Processing and Recycling of Non-Ferrous Metal, School of Materials Science and Engineering, Lanzhou University of Technology, Lanzhou 730050, China; lzy08181943@163.com (Z.L.); chengbo@lut.edu.cn (B.C.)

<sup>3</sup> School of Mechanical Science and Technology, Belarus National Technical University, 220013 Minsk, Belarus; vvvcoatign@yandex.ru (V.V.); georggoran@rambler.ru (G.G.)

\* Correspondence: liws@lut.edu.cn (W.L.); 101113920@163.com (G.A.)

**Abstract:** Laser scanning modification was applied to secondarily melt the top ceramic coating surface of lanthanum zirconate/yttria-stabilized zirconia double ceramic thermal barrier coatings (LZO/YSZ TBCs) to reduce the gas oxygen diffusion and improve the TBCs service life. Isothermal oxidations with different times were carried out on the as-sprayed (AS) TBCs and laser-remolten (LR) TBCs at 1100 °C to investigate thermally growth oxide (TGO) growth mechanisms and isothermal oxidation behaviors. The results showed that the laser-remolten top-ceramic-coating dense layer with a columnar crystal structure of LR TBCs presented a 96.3% and 59.1% lower surface roughness and porosity, respectively, than those of the top ceramic coating of AS TBCs, and the TGO growth rate of LR TBCs decreased by 46.2% compared to that of AS TBCs. The mixed-oxides appearance time of LR TBCs (50 h) was later than that of AS TBCs (25 h). After 100 h of isothermal oxidation, the total TGO thickness of LR TBCs was only 77.2% of that of AS TBCs, and the effects of the laser-remolten TBCs on gas oxygen diffusion inhibition and high-temperature oxidation resistance were promising in LZO/YSZ TBCs.

**Keywords:** LZO/YSZ TBCs; laser-remolten layer; isothermal oxidation; TGO growth; oxidation resistance



**Citation:** Li, W.; Li, Z.; An, G.; Cheng, B.; Song, Q.; Sun, J.; Vaganov, V.; Wang, C.; Goransky, G. Isothermal Oxidation TGO Growth Behaviors of Laser-Remolten LZO/YSZ Thermal Barrier Coatings. *Coatings* **2022**, *12*, 107. <https://doi.org/10.3390/coatings12020107>

Academic Editors: Damian Przystacki and Michal Kulka

Received: 11 December 2021

Accepted: 14 January 2022

Published: 18 January 2022

**Publisher's Note:** MDPI stays neutral with regard to jurisdictional claims in published maps and institutional affiliations.



**Copyright:** © 2022 by the authors. Licensee MDPI, Basel, Switzerland. This article is an open access article distributed under the terms and conditions of the Creative Commons Attribution (CC BY) license (<https://creativecommons.org/licenses/by/4.0/>).

## 1. Introduction

Thermal barrier coatings (TBCs) are widely used in hot end components of gas turbines, such as combustion chambers and high-pressure nozzles, to protect hot end components from oxidation, thermal corrosion, erosion wear, and even touch-friction between blades. Ultimately, the service life and continuous work efficiency of the hot end components has been improved [1–5]. Typical TBCs are composed of ceramic coatings, metallic bonding coatings, superalloy substrates, and thermally growth oxide (TGO) layers. The most widely used ceramic coating is 6 wt.%~8 wt.% yttria partially stabilized zirconia (YSZ) for its high thermal expansion coefficient ( $11 \times 10^{-6} \text{ k}^{-1}$ ), low thermal conductivity ( $2.1 \text{ W} \cdot \text{m}^{-1} \cdot \text{k}^{-1}$ ), and satisfactory phase stability [6,7]. NiCoCrAlY is one of the most common choices for aero engine blade bonding coatings, because it not only improves the adhesion between the ceramic top layer and substrate, but also has excellent oxidation resistance and thermal resistance [8,9]. The TGO layer, which usually consists of a continuous dense  $\text{Al}_2\text{O}_3$  layer and mixed-oxides layer [10–12], is formed during the bonding coating oxidation because oxygen continuously passes through the ceramic coating in the TBC high-temperature service process.

The degradation of TBCs involves many factors, such as high-temperature oxidation, thermal shock, hot corrosion, and corrosive wear [13,14]. Among them, the spalling failure of TBCs under high temperature is closely related to the thickness, growth rate, and composition of TGO. Dong et al. [15] reported that there is a linear relationship between the TGO strain energy and its thickness, and the continuous thickening of TGO could cause serious cracking and spalling of ceramic coatings in TBCs. Bai et al. [16] showed that the  $\text{Al}_2\text{O}_3$  layer formation decreased the TGO growth rate at the initial oxidation stage, but when the  $\text{Al}_2\text{O}_3$  layer was consumed by mixed-oxides formation, and resulted in a sharply increased TGO growth rate, the TBCs were close to the critical failure state. Once more, during the formation of TGO, large-volume mixed oxides are the reason for the shortening of the TBC service life, so the study of TGO is particularly important in the process of high-temperature oxidation. TGO formation processes are mainly affected by oxygen diffusion mechanisms of oxygen transporting from the outside to the bonding coating of TBCs [17–19]; for example, the gas oxygen diffusion of  $\text{O}_2$  propagates through pores and microcracks in ceramic coatings, and the ion oxygen diffusion of  $\text{O}^{2-}$  migrates through the lattice of ceramic coating materials. Fox [20] reported that the gas oxygen diffusion through the top ceramic coating is considered to be the main determinants of oxygen transport in blade TBCs in a gas turbine servicing process.

To further delay TGO formation and growth by inhibiting oxygen diffusion, double-ceramic-layer TBCs were proposed [21] through the deposition of an additional ceramic coating with low oxygen ion diffusivity on the surface of traditional single-layer YSZ TBCs. For example,  $\text{La}_2\text{Zr}_2\text{O}_7$  (LZO) is one of the most promising candidates for oxygen barrier TBC layer materials, for its excellent oxygen ion conductivity ( $9.2 \times 10^{-4}$  S/cm, 1000 °C), which is approximately three orders of magnitude lower than that of YSZ (0.1 S/cm, 1000 °C) [22]. Liu et al. [23] prepared LZO/YSZ double-ceramic-layer TBCs by air plasma spraying (APS) and electron beam physical vapor deposition (EB-PVD), and they proved that LZO is an effective oxygen ion barrier material under high-temperature oxidation working conditions. Wang's [24] and Xu's [25] high-temperature oxidation experiments showed that, due to its beneficial effect on preventing ion oxygen diffusion, LZO/YSZ double-ceramic-layer TBCs have a longer working life than the traditional YSZ TBCs.

Reducing APS coating defects is also an effective way to slow down the migration rate of oxygen ions in TBCs, and laser remelting has been considered one of the effective methods. Laser-remelting treatment of YSZ TBCs was proposed and prepared by Zaplatynsky et al. [26], who revealed that the laser remelting would provide the YSZ TBCs surface with high smoothness and reduced permeability. Thereafter, much research was carried out on laser-remolten APS coatings, and it was found that the laser-remolten columnar structure of the YSZ APS coating had a certain effect on the pores' sealing and the surface hardness improvement [27–31], and it was beneficial to prolong the coating life. Ahmadi-Pidani et al. [32] and Fretias [33] used pulsed lasers to treat plasma-sprayed ceria and yttria-stabilized zirconia (CYSZ) TBCs, and the effects of laser remelting on the microstructure and thermal shock resistance of the coatings were evaluated; the results showed that the lifetime of the laser-treated TBCs was enhanced about fourfold. This is attributable to the formation of a continuous network of segmented cracks perpendicular to the surface and the increase in strain accommodation. Further, the effects of laser remelting treatment on the formation and growth mechanism of TGO, especially on the double-ceramic-layer TBCs, are desired.

In the present work, laser scanning for remelting modification on LZO/YSZ double-ceramic-layer TBCs was carried out, and the remelting effects on the microstructure, TGO growth behavior, and oxidization mechanism were investigated, to explore the sealing feasibility to reduce oxygen transport and improve the high-temperature service life of LZO/YSZ double-ceramic-layer APS TBCs.

## 2. Experimental Procedure

### 2.1. Materials and Sample Preparation

NiCoCrAlY powder (Amdry 365-2, Oerlikon Metco) with a particle size of 45–75  $\mu\text{m}$  was the feedstock of the bonding coating. 8YSZ powder (Metco 204B-NS, Oerlikon Metco) with a particle size of 35–86  $\mu\text{m}$  and LZO (Hunan Zhaoyi Thermal Spraying Material Co., Ltd., Yiyang, China) with a particle size of 12–47  $\mu\text{m}$  were feedstocks of the inner ceramic coating and outer ceramic coating, respectively. The Inconel 738 substrate with a size of 100 mm  $\times$  20 mm  $\times$  12 mm was sandblasted, alcohol-ultrasonically cleaned, dried, and preheated to 150  $^{\circ}\text{C}$ . The bonding coating, the inner ceramic coating, and the outer ceramic coating were deposited successively by Sulzer Metco 9MB plasma spraying with an interval less than one hour between the spraying of each coating, and the spraying parameters are shown in Table 1. A IPG YLS-4000 fiber laser with a maximum output power of 4000 W and wavelength of 1070 nm was applied for laser scanning remelting treatment on the plasma-sprayed sample surface, and the scanning process was protected by argon. The laser scanning parameters are shown in Table 2.

**Table 1.** Parameters of air plasma spraying process.

Parameters	NiCoCrAlY	YSZ	LZO
Voltage (V)	55	60	60
Current (A)	500	650	650
Spray distance (mm)	15	10	10
Primary gas flow, Ar (L/min)	15	15	15
Secondary gas flow, H <sub>2</sub> (L/min)	9	9	9
Powder feed rate (g/min)	33	30	30

**Table 2.** Parameters of laser scanning process.

Power (W)	Scanning Speed (mm/s)	Defocus Amount (mm)	Spot Size (mm)	Overlap Rate	Energy Ratio (J)
100	20	+15	3	30%	1.67

### 2.2. Isothermal Oxidation and Characterization

The prepared as-sprayed (AS) and laser remolten (LR) TBCs samples were cut into 10 mm  $\times$  10 mm  $\times$  12 mm by a diamond wire saw and put in a muffle furnace at room temperature. Then, the muffle furnace was heated to 1100  $^{\circ}\text{C}$  at a heating rate of 5  $^{\circ}\text{C}/\text{min}$  and isothermally oxidized for 10, 25, 50, and 100 h, and the furnace was then cooled down to room temperature. The oxidation weight increase of the samples was weighted by an analytical balance with  $\pm 0.0001$  g accuracy, and three samples in each group were taken to obtain the mean value of the oxidation weight gain.

An LSM-800 laser confocal microscope and D/MAX 2500 PC X-ray diffractometer (XRD, Rigaku, Tokyo, Japan) were used to characterize the surface roughness and phase. To obtain the same level of XRD diffractograms, samples were polished by sandpaper to the same roughness standard. To obtain the XRD pattern of TGO, the samples after 100 h of oxidation were carefully mechanically ground to the ceramic coating/NiCoCrAlY interface against the coating growth direction. Microstructural characterizations of the surface and cross-section were analyzed by QUANTA FEG 450 scanning electron microscopes (SEM, Thermo Fisher Scientific, Berlin, Germany) equipped with X-ray energy-dispersive spectroscopy (EDS, Thermo Fisher Scientific, Berlin, Germany). Porosity and TGO thickness were measured by Image Pro Plus 6 software from 10 SEM images with the same magnification at different areas.

### 3. Results and Discussion

#### 3.1. Coating Microstructure

Figure 1 shows the surface morphology of AS and LR TBCs. As shown in Figure 1a, there are partially unmolten particles, protrusion areas, microcracks, and voids on the AS TBCs surface. These typical characteristics of APS coatings are attributed to the unevenly melted particles under inhomogeneous plasma flame heating. Fully melted powders with high kinetic energy are accumulated on the substrate surface with a flat shape, and the protrusions are generated with the continuously accumulated partly melted particles [28]. Meanwhile, microcracks generate from the stress concentration of the high cooling rate, holes and voids are produced from an insufficient overlap and residual gas, and a rough surface and the looser microstructure are presented. The AS TBCs surface roughness is  $10.8 \mu\text{m}$  ( $S_a$ ), as shown in Figure 1b, and it may increase the oxygen contact area and accelerate the interface oxidation reaction between the ceramic coating and bonding coating [34]. As shown in Figure 1c, the LR TBC surface is smooth and flat, except for the network cracks generated from the laser scanning melting and Ar rapid cooling [35], and the roughness decreases to  $0.4 \mu\text{m}$  ( $S_a$ ), as shown in Figure 1d.

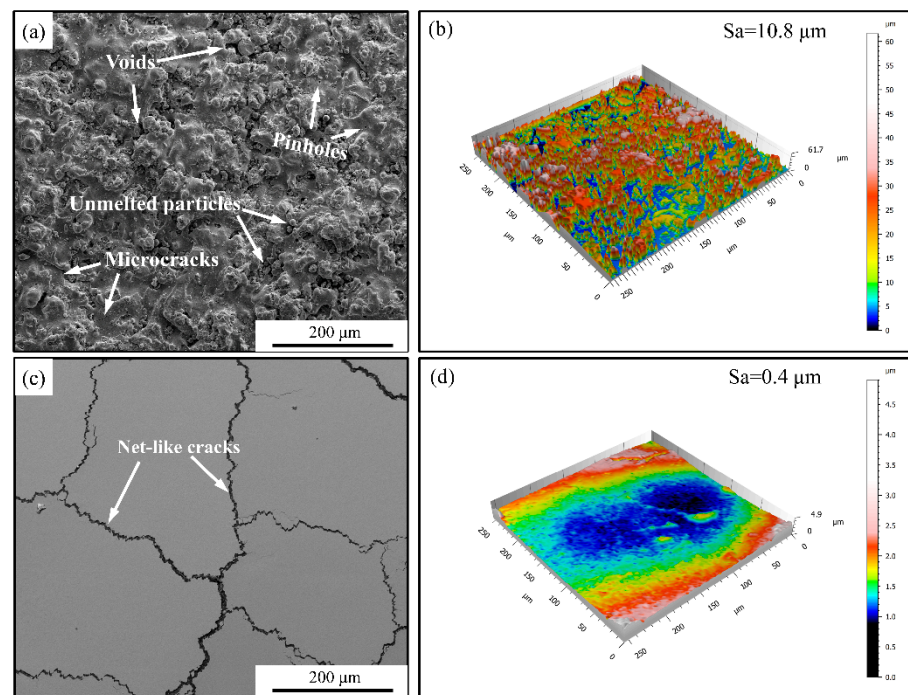


**Figure 1.** Surface morphology of TBCs: (a) AS, (b) AS surface roughness, (c) LR, and (d) LR surface roughness.

Figure 2 shows the AS and LR TBCs cross-sectional morphology. Figure 2a shows that the AS TBCs are composed by an outer ceramic coating (LZO), an inner ceramic coating (YSZ), and a metallic bonding coating (NiCoCrAlY) with corresponding thicknesses of  $150 \pm 20 \mu\text{m}$ ,  $120 \pm 20 \mu\text{m}$ , and  $100 \pm 20 \mu\text{m}$ , respectively. The outer ceramic coating cross-section of the as-sprayed LZO is a typical lamellar structure, with a large number of splats and a high porosity of 11.5% (as shown in Figure 2b). Meanwhile, Figure 2c shows that there is a dense remolten layer of LZO with a thickness of about  $100 \mu\text{m}$  at the outer ceramic coating cross-section in LR TBCs, and the porosity is 4.7%, which is only 40.9% of that in the AS outer ceramic coating. Cracks perpendicular to the coating surface, that is, occurring during the as-spray layered structure, transform to a columnar structure along the heat dissipation direction by the laser melting and rapid cooling. The outer ceramic coating of LR TBCs has a structure combination of remolten dense columnar and sprayed

porous, which is beneficial in inhibiting the external oxygen diffusion, as well as enhancing the TBC's thermal stability because of the resulting strain tolerance improvement [35,36].

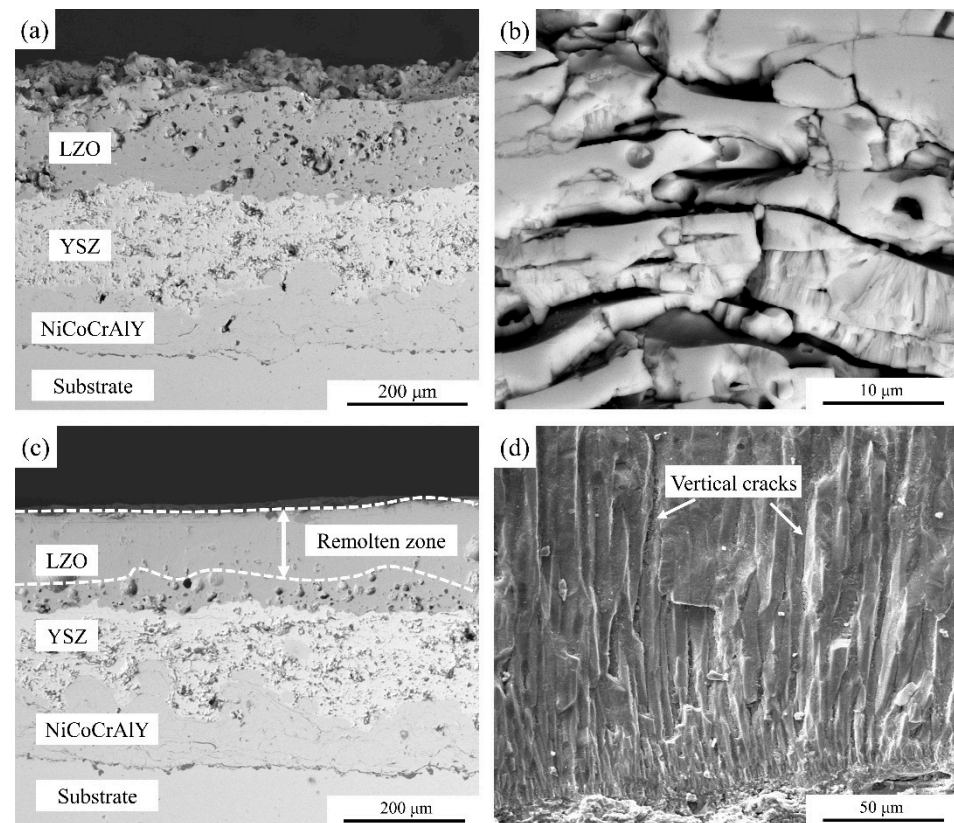
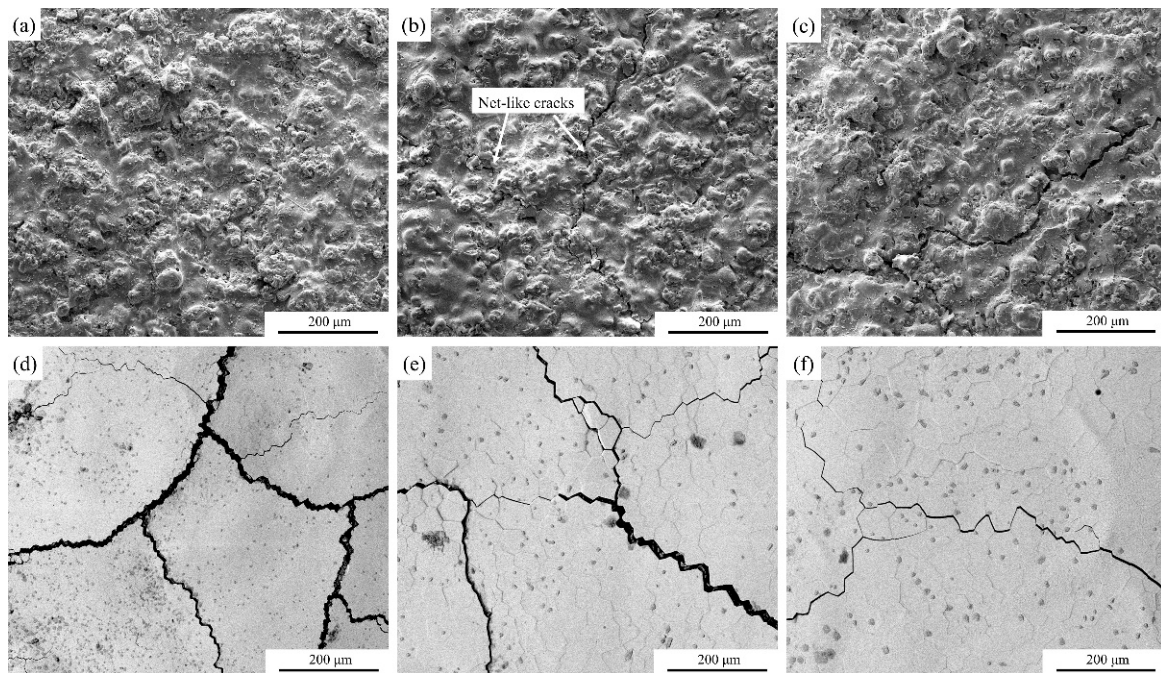


**Figure 2.** Cross-sectional morphology of TBCs: (a) AS, (b) AS LZO outer ceramic layer, (c) LR, and (d) LR LZO outer ceramic layer.

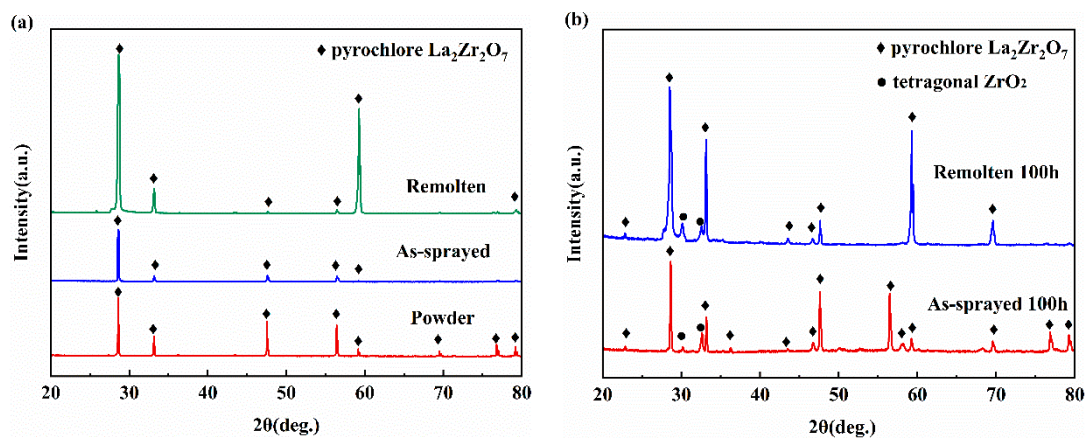
Figure 3 shows the surface morphology of AS and LR TBCs isothermally oxidized at 1100 °C for 25, 50, and 100 h. As shown in Figure 3a, after isothermal oxidation for 25 h, the AS TBCs surface is rough, and the pinholes and microcracks increase. The pinholes on the surface of AS TBCs increase continuously after 50 h of isothermal oxidation, and microcracks seem to expand and connect into net-like cracks, as shown by the white arrow in Figure 3b. These defects aggravate the oxygen transport and is harmful to the TBC oxidation resistance. After 100 h of isothermal oxidation, more unmolten powder particles fall off the AS TBCs surface and there are more pinholes; and the pinholes and the wider connecting cracks become enlarged, as shown in Figure 3c. Meanwhile, for the LR TBCs, with the isothermal oxidation time extended to 100 h, the coating surface remains smooth and dense, as shown in Figure 3d–f, and is conducive to the high-temperature oxidation resistance of TBCs.

Figure 4 shows XRD patterns of the LZO powder, AS, and LR TBCs before and after the 100 h isothermal oxidation. Figure 4a shows that the LZO powder and two kinds of TBC LZO surface phases before isothermal oxidation are all pyrochlore structures, and a higher diffraction intensity is presented in LR TBCs for its preferred orientation of crystals [37] that was rearranged from lamellar to columnar by the laser remelting process (as shown in Figure 2b,d). Figure 4b shows that both AS and LR TBC LZO surface phases after 100 h of isothermal oxidation are tetragonal ZrO<sub>2</sub> with a low-intensity diffraction peak, although the major diffraction peak still corresponds to the pyrochlore structure. The tetragonal ZrO<sub>2</sub> phase formation is attributed to the preferential volatilization of La<sub>2</sub>O<sub>3</sub> during the long-time oxidation at high temperature, and thus, the stoichiometric inhomogeneity forms in LZO [38]. This is not the reason for the LZO/YSZ TBC's failure during the high-temperature

service, so the influence of the ceramic coating phase transformation on high-temperature oxidation resistance can be negligible [39].



**Figure 3.** Surface morphology of 1100 °C isothermally oxidized TBCs against time: (a) AS 25 h, (b) AS 50 h, (c) AS 100 h, (d) LR 25 h, (e) LR 50 h, and (f) LR 100 h.



**Figure 4.** XRD patterns: (a) LZO powder, AS, and LR TBCs, and (b) AS and LR TBCs isothermally oxidized for 100 h at 1100 °C.

### 3.2. TGO Growth Kinetic

The weight gain after different times of isothermal oxidation at 1100 °C is calculated by Equation (1):

$$\Delta G = (m_2 - m_1) / S \quad (1)$$

where  $\Delta G$  is the oxidation weight gain mass per unit area;  $m_2$  is the weight of samples after isothermal oxidation;  $m_1$  is the weight of samples before isothermal oxidation;  $S$  is the initial surface area of samples. Figure 5 shows the 1100 °C isothermal oxidation weight gain curves against time of AS and LR TBCs. After 10 h of isothermal oxidation, the weight gains of AS TBCs and LR TBCs are 1.674 and 1.853 mg/cm<sup>2</sup>, respectively, attributed to the network cracks in LR TBCs (Figure 1c), providing more channels for oxygen rapid diffusion

from the outer ceramic coating to the metallic bonding coating; and the weight gain of LR TBCs is higher than that of AS TBCs. From then on, the weight gain rate of both AS and LR TBCs obviously slows down, and after 25 h, the oxidation weight gain of LR TBCs is obviously lower than that of AS TBCs. After 100 h, the weight gains of AS TBCs and LR TBCs are 4.215 and 3.841 mg/cm<sup>2</sup>, respectively. As, when the long-time high-temperature isothermal oxidation extends, the network cracks in LR coating gradually heal, as shown in Figure 3d–f, it reduces oxygen-permeating channels in ceramic coatings and further postpones the oxidation growth [40].

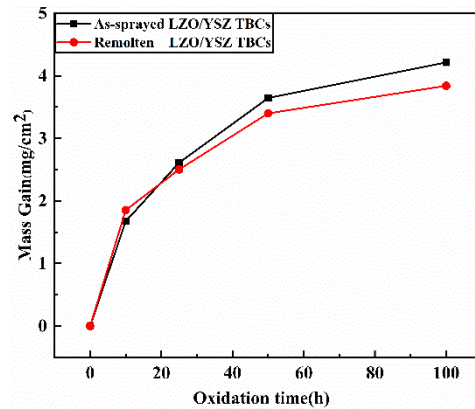


Figure 5. Weight gain curve of isothermal oxidation at 1100 °C.

Figure 6a shows the TGO thickness variation curves of AS and LR TBCs that were isothermally oxidized at 1100 °C for 100 h. Two TGO growth stages, the rapid growth stage and the steady growth stage, are presented. Within the first 10 h isothermal oxidation period, as Figures 1 and 2 shows, the protrusion areas, microcracks, and voids in the AS TBCs and the network cracks in LR TBCs are all in favor of oxygen permeation and negative to TBC high-temperature oxidation resistance, resulting in TGO forming quickly along the interface of the ceramic coating and bonding coating. The TGO average thicknesses of AS and LR TBCs are 1.746 and 1.966 μm, respectively. In the period from 10 to 100 h of isothermal oxidation, a steady TGO growth stage is presented; although the TGO growth rate slows down, the TGO average thicknesses of AS and LR TBCs are 4.590 and 3.542 μm, respectively, after 100 h of isothermal oxidation.

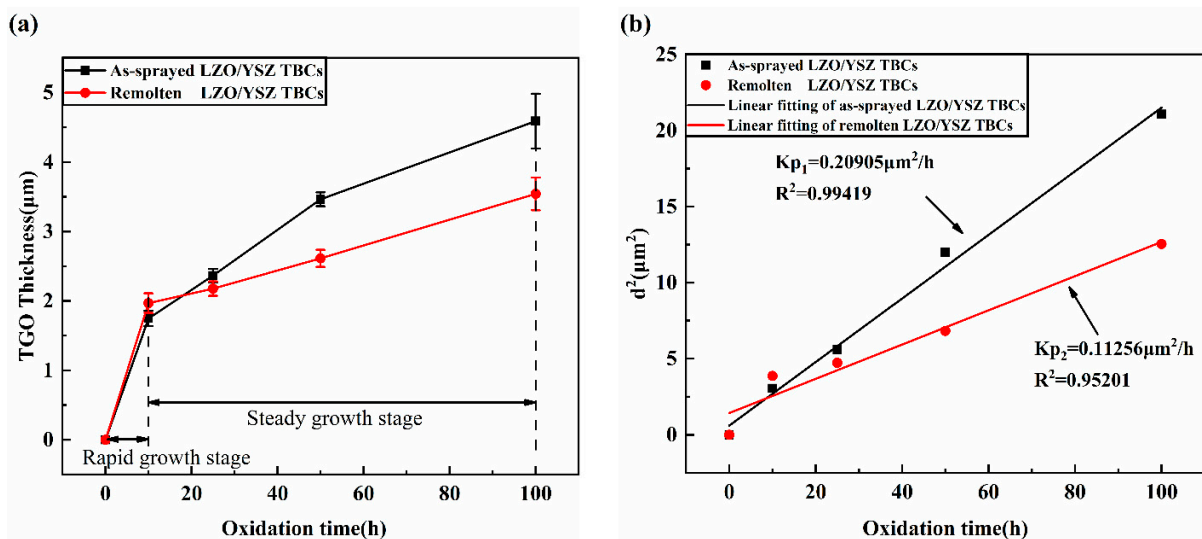


Figure 6. Isothermal oxidation kinetics curves at 1100 °C of (a) TGO thickness and (b) the fittings growth rate constants  $K_p$ .

Figure 6b shows the TGO growth rate constant  $K_p$  values by fitting the TGO thickness growth of AS and LR TBCs, respectively, according to the following Equation (2) [41]:

$$d^2 = K_p \times t + c \quad (2)$$

where  $d$  is the thickness of the TGO layer,  $K_p$  is the growth rate constant of TGO,  $t$  is the oxidation time, and  $c$  is a constant.  $K_p$  presents a parabolic law, and the  $K_p$  of AS and LR TBCs are 0.20905 and 0.11256  $\mu\text{m}^2/\text{h}$ , respectively, and indicates that the oxidation rate of LR TBCs decreases by 46.2% more than that of AS TBCs. It is generally believed that the greater the TGO thickness produced, the greater the TGO growth stress accumulated, and the shorter the TBC service life achieved [2]. The dense laser remolten layer has a crucial effect on inhibiting TGO growth, as well as further decreasing the TBC oxidation rate.

### 3.3. TGO Morphology and Composition Characterization

Figure 7 shows the TGO morphology of AS and LR TBCs isothermally oxidized at 1100 °C for 10, 25, 50, and 100 h. After isothermal oxidization for 10 h, Figure 7a,b show that a uniform and continuous black TGO layer is formed along the ceramic/bonding coating interface in both the AS and LR TBCs. After isothermal oxidization for 25 h, Figure 7c,d show that a few gray oxides (shown by dotted line in Figure 7c) appear on the side of the black oxide TGO layer of AS TBCs; however, the TGO of LR TBCs remains as a single black oxide layer. After isothermal oxidization for 50 h, Figure 7e,f show that a clear double TGO layer structure appears in AS TBCs, as well as continuous gray oxides on the upper part and a black oxide layer on the lower part. Simultaneously, a small amount of discontinuous gray oxides (shown by the dotted line in Figure 7f) appears on the side of the black oxide TGO layer of LR TBCs, and the TGO thickness of both AS and LR TBCs increases obviously. After isothermal oxidization for 100 h, Figure 7g shows that the thickness of the continuous gray oxides TGO layer of AS TBCs significantly increases, many inner pores appear, and the thickest TGO area reaches 12  $\mu\text{m}$ . While the TGO thickness of LR TBCs is obviously smaller than that of AS TBCs, the increase rate of LR TBCs is lower than that of AS TBCs, and a thinner gray oxides layer with fewer inner pores inside begins to appear in LR TBCs, as shown in Figure 7h. A continuous thickening of TGO accompanied by the accumulation of stress formed during the isothermal oxidation process, and the failure of most TBCs was closely related to the growth of TGO and the variation in stress in TGO [41].

Figure 8a,b show EDS element mappings of the yellow rectangular area in Figure 7c,d of AS and LR TBCs that are isothermally oxidized for 25 h. The AS TBCs TGO exhibits a double-layer structure of a small continuous gray mixed-oxides layer on the upper part and black  $\text{Al}_2\text{O}_3$  layer on the lower part, and the mixed oxides are composed of oxides of Ni, Co, and Cr. The LR TBCs TGO remains as a single  $\text{Al}_2\text{O}_3$  layer.

Figure 9a,b show the enlarged TGO morphology of the yellow rectangular area in Figure 7g,h of AS and LR TBCs that are isothermally oxidized for 100 h. From Figure 9c, the corresponding EDS line-scan profile along the yellow arrow line in Figure 9a, one can see that the AS TBC TGO exhibits a double-layer structure of large continuous gray mixed oxides on the upper part and a small black  $\text{Al}_2\text{O}_3$  layer on the lower part. In addition, from Figure 9d, the corresponding EDS line-scan profile along the yellow arrow line in Figure 9b, the LR TBCs TGO exhibits a double-layer structure of an uneven and discontinuous gray mixed-oxides layer on the upper part and black  $\text{Al}_2\text{O}_3$  layer on the lower part, and it seems that the continuous mixed oxides appear. Meanwhile, the intensities of Ni, Co, and Cr in LR TBCs remain lower than those in AS TBCs, and Al is higher in LR TBCs according to the EDS point analysis of point 1 (Al = 19.1%, Ni = 13.2%, Co = 10.5%, Cr = 11.2%, at%) and point 2 (Al = 38.5%, Ni = 2.2%, Co = 3.3%, Cr = 2.9% at%). This reveals that  $\text{Al}_2\text{O}_3$  in both AS and LR TBCs TGO was consumed and transferred to  $\text{CoCr}_2\text{O}_4$ ,  $(\text{Ni}, \text{Co})\text{Al}_2\text{O}_4$ ,  $\text{NiCr}_2\text{O}_4$ , and  $\text{NiO}$  mixed spinel oxides. Laser scanning remelting is promising in inhibiting the formation of mixed spinel oxides from keeping the TGO structure as a single  $\text{Al}_2\text{O}_3$  layer for a long time.

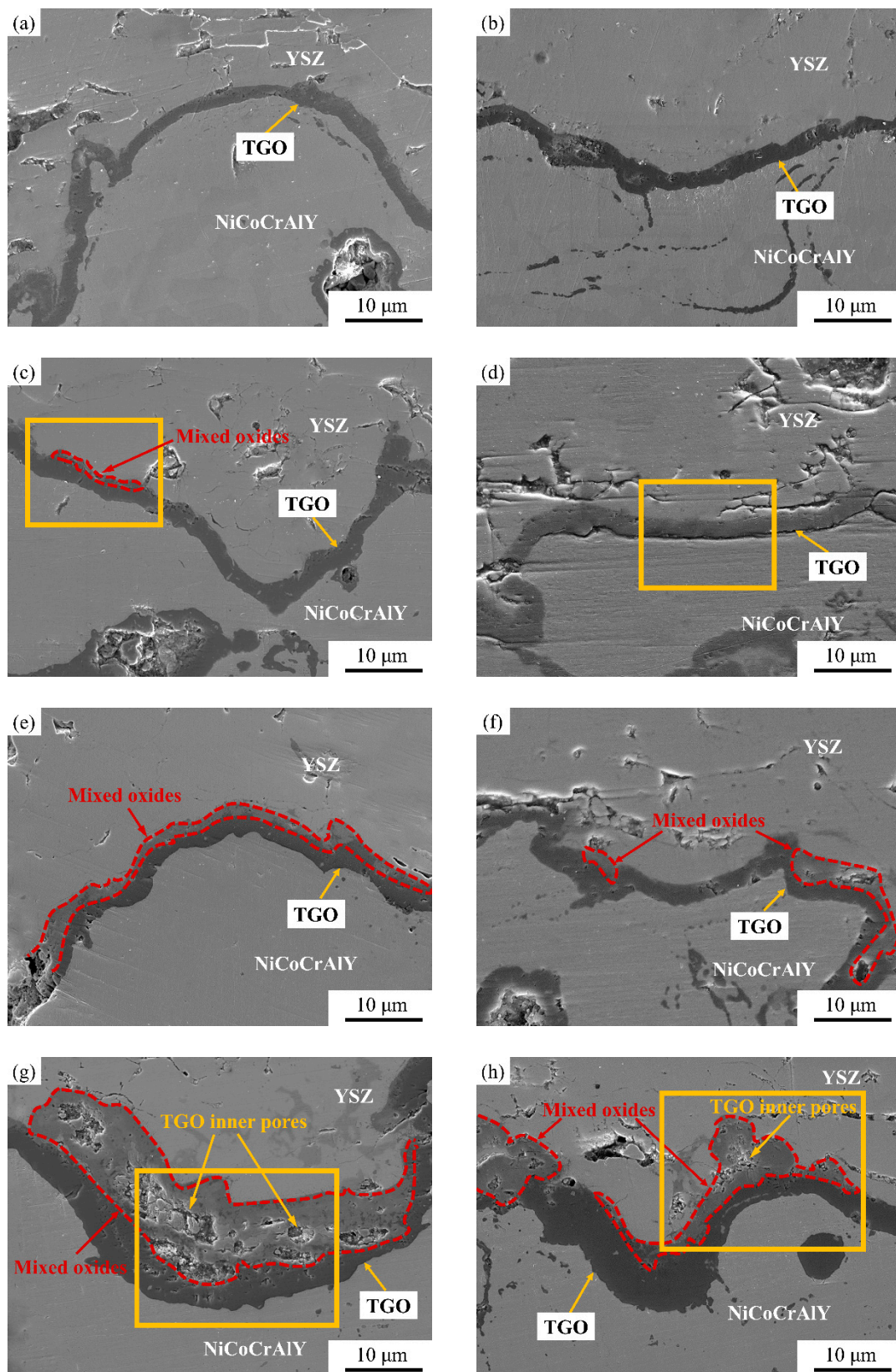


**Figure 7.** TGO morphologies of TBCs isothermally oxidized at 1100 °C for different times: (a) AS 10 h, (b) LR 10 h, (c) AS 25 h, (d) LR 25 h, (e) AS 50 h, (f) LR 50 h, (g) AS 100 h, and (h) LR 100 h.

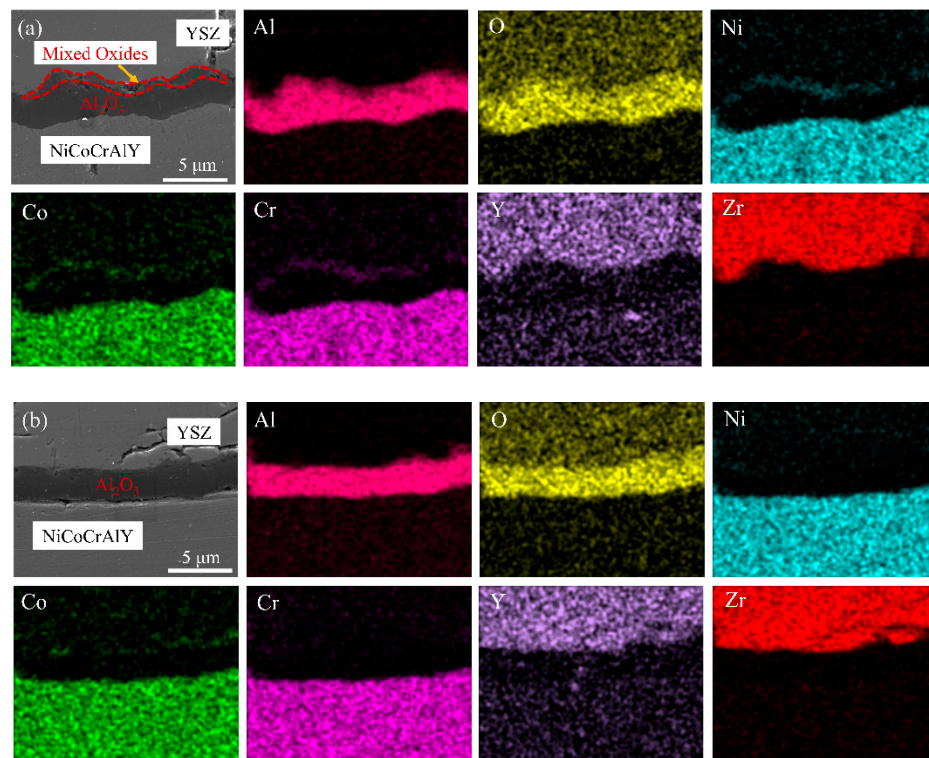


Figure 8. EDS mapping profiles of TGO by oxidation at 1100 °C for 25 h: (a) AS TBCs and (b) LR TBCs.

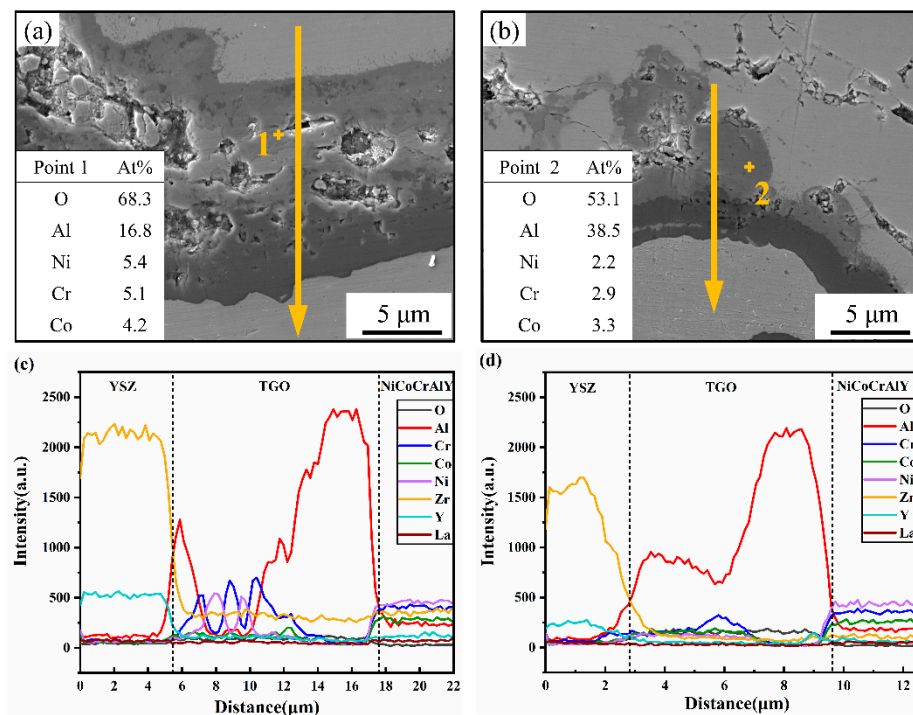
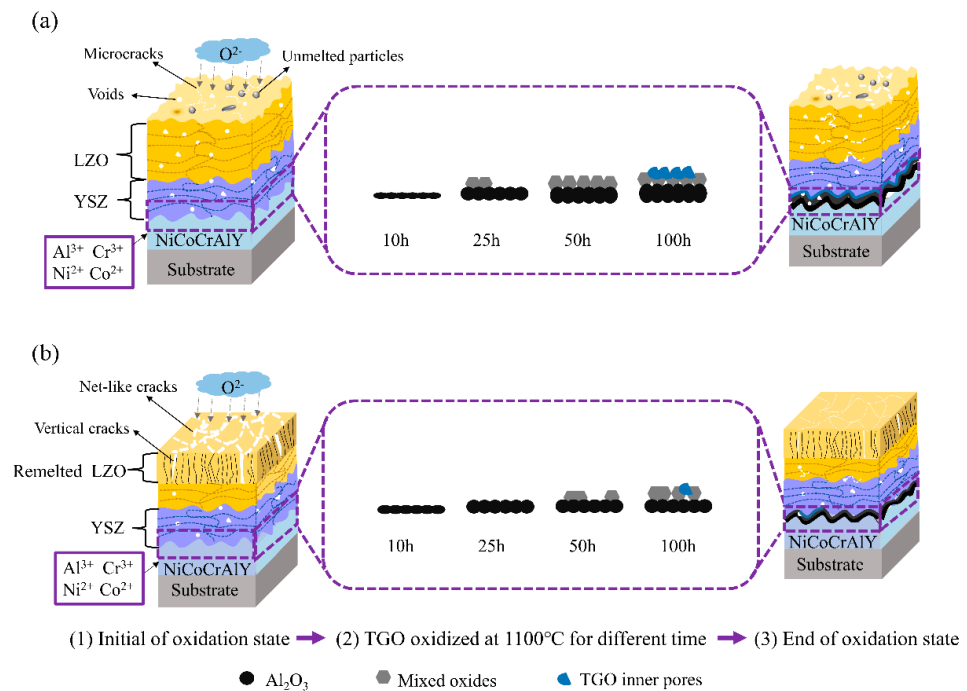


Figure 9. EDS line-scan profiles of TGO by oxidation at 1100 °C for 100 h: (a,c) AS TBCs and (b,d) LR TBCs.

### 3.4. Oxidation Behavior and Mechanism

Figure 10 shows a schematic illustration of the AS and LR TBC oxidation mechanisms. The TGO thickness evolution of both TBCs during the different times of isothermal oxidation at 1100 °C is shown in the amplified violet rectangular frame. According to Figures 1a and 2a,b, Figure 10a also shows that there are protrusion areas, microcracks,

and voids on the AS TBC surface and a typical lamellar structure with high porosity in its cross-section. According to Figures 1c and 2c,d, Figure 10b also shows that the LR TBC surface presents a smooth surface with net-like cracks and vertical cracks because the laser scanning remelting had eliminated the surface defects of AS TBCs. The left side of Figure 10 shows the initial oxidation state of both the AS and LR TBCs.



**Figure 10.** Schematic illustration of oxidation mechanism: (a) AS LZO/YSZ TBCs and (b) LR LZO/YSZ TBCs.

A dense and continuous  $\text{Al}_2\text{O}_3$  layer is the most desirable oxide scale in the TGO due to its low oxygen diffusivity, superior adherence, and lower growth rate [42], which serves as a diffusion barrier to retard the Al depletion, reduce the tendency of the outward diffusion through TGOs of other metallic cations, decrease the TGO growth rate, and prevent the formation and growth of spinel, and the coatings with a larger Al content have a longer service life [43]. After oxidation for 10 h,  $\text{Al}^{3+}$  in both the AS and LR TBCs first diffuses outward from the metallic bonding coating to the interface and reacts with  $\text{O}^{2-}$  to form  $\text{Al}_2\text{O}_3$  due to the lowest Gibbs free energy needed, as shown in Table 3. The vertical cracks in LR TBCs provided more oxygen-permeated channels to the ceramic coating and bond coating interface, so the  $\text{Al}_2\text{O}_3$  thickness of LR TBCs is slightly larger than that of AS TBCs at this initial oxidation stage. After oxidation for 25 h, the  $\text{Al}^{3+}$  content in the metallic bonding coating of AS TBCs decreases under the critical concentration, and  $\text{Ni}^{2+}$ ,  $\text{Cr}^{3+}$ , and  $\text{Co}^{2+}$  begin to diffuse through the  $\text{Al}_2\text{O}_3$  layer to participate in oxidation; thus,  $\text{NiO}$ ,  $\text{Cr}_2\text{O}_3$ , and  $\text{CoO}$  are formed. As  $\text{NiO}$ ,  $\text{Cr}_2\text{O}_3$ , and  $\text{CoO}$  are unstable at high temperature [44], they will spontaneously react with  $\text{Al}_2\text{O}_3$  to form  $(\text{Co}, \text{Ni})\text{Cr}_2\text{O}_4$  and  $(\text{Ni}, \text{Co})\text{Al}_2\text{O}_4$  spinel oxides via reactions (3) and (4), and the discontinuous mixed oxides will appear.

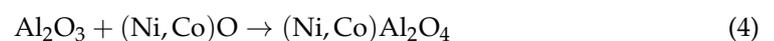
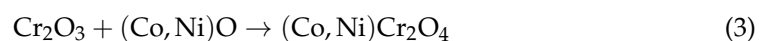


**Table 3.** Gibbs free energy of different oxides [45,46].

Oxides	Al <sub>2</sub> O <sub>3</sub>	Cr <sub>2</sub> O <sub>3</sub>	NiO	CoO
1373 K, $\Delta G^\theta$ (kJ/mol)	−1239.1	−769.6	−122.8	−135.7

However, the TGO thickness of LR TBCs increased slightly and kept the single Al<sub>2</sub>O<sub>3</sub> layer, which indicates that less oxygen arrived at the bonding coating of LR TBCs for the net-like cracks and vertical cracks healed. In addition, oxygen-permeated channels were reduced in ceramic coatings and the TGO growth in LR TBCs was further postponed, because the thermal stress concentration during high-temperature oxidation would be released by the vertical microcracks, as shown in Figure 2d [47], which had already existed in the remolten zone of the outer ceramic coating before oxidation, as shown in Figure 1c, which could also release part of the thermal stress during thermal fatigue. On the other hand, with the help of crack healing, the damage induced by thermal stress was effectively decreased in LR TBCs. The oxidation rate in LR TBCs was obviously lower than that in AS TBCs, as shown in Figure 6b.

After oxidization for 50 h, the TGO of AS TBCs maintained the high growth rate, and the thicker upper mixed-oxides layer on the lower Al<sub>2</sub>O<sub>3</sub> layer of the TGO double-layer structure continuously formed. For the LR TBCs, there was increasingly more oxygen diffusing into the ceramic coatings and being accumulated slowly and steadily over time to the interface between the ceramic coating and bonding coating, although the high temperature healed the oxygen-rapidly transferring channel of the network cracks and vertical cracks in the LR TBCs, as shown in Figure 3e, and, as a result, the discontinuous mixed oxides started to appear.

After oxidization for 100 h, an obvious double-layer structure TGO formed completely in both the AS and LR TBCs, and the TGO thicknesses both increased obviously. For the AS TBCs, a nearly 70% thickness proportion of TGO was the mixed oxides, and the inner pores formed and accumulated in the mixed-oxides region of TGO. For the LR TBCs, a nearly 80% thickness proportion of the dense and continuous black Al<sub>2</sub>O<sub>3</sub> layer was still present (as shown in Figures 7h and 9b); however, the uneven and discontinuous gray mixed-oxides layer with small inner pores appeared for such a long-time high-temperature oxidation. The TGO presented more inner pores and a larger thickness of mixed oxides in AS TBCs because the as-sprayed LZO could not prevent the oxygen diffusion, correspondingly, under the beneficial effect of oxygen insulation from the laser-remolten LZO structure in LR TBCs, as shown in Figures 2d and 3f. This indicates that LR TBCs had a better oxidation resistance.

Figure 11 shows XRD patterns obtained from the ceramic coating/NiCoCrAlY interface of AS TBCs and LR TBCs after 100 h of isothermal oxidation. For AS TBCs, the dominant interface phases were Cr<sub>2</sub>O<sub>3</sub>, (Ni, Co) (Al, Cr)<sub>2</sub>O<sub>4</sub> and a small amount of NiO. For LR TBCs, the main phases were Ni<sub>3</sub>Al, Al<sub>2</sub>O<sub>3</sub>, and a small amount of Cr<sub>2</sub>O<sub>3</sub> and (Ni, Co) (Al, Cr)<sub>2</sub>O<sub>4</sub>. This is consistent with the TGO growth trend in Figures 7 and 9. A dense and continuous Al<sub>2</sub>O<sub>3</sub> layer played a positive role on the TGO performances, such as slower growth rate, good adhesion [44], and further oxidation protection on TBC at high temperature, so the Al<sub>2</sub>O<sub>3</sub> layer was the most desirable oxide scale of TGO [48]. However, TGO will transfer from a single Al<sub>2</sub>O<sub>3</sub> layer to double layers of Al<sub>2</sub>O<sub>3</sub> + Cr<sub>2</sub>O<sub>3</sub>, (Ni, Co) (Cr, Al)<sub>2</sub>O<sub>4</sub>, and NiO mixed oxides [45], and the presence of mixed oxides will reduce the interfacial toughness of TGO and will have a negative effect on the coating life. Doleker [44] reported that the protection effect of the lower black Al<sub>2</sub>O<sub>3</sub> layer was close to failure when the TGO formed a continuous mixed-oxide layer with the inner pores. To summarize, the Al<sub>2</sub>O<sub>3</sub> layer thickness of TGO in both groups of TBCs increased with isothermal oxidation time and then decreased slowly with the appearance and growth of the adverse multilayer structure Cr<sub>2</sub>O<sub>3</sub>, (Ni, Co) (Cr, Al)<sub>2</sub>O<sub>4</sub>, and NiO mixed oxides. In addition, the thickness proportion of Al<sub>2</sub>O<sub>3</sub> in the total TGO layer in LR TBCs always remained greater than that in AS TBCs after isothermal oxidation for 10 h. That is to say that laser scanning remelting

is promising in inhibiting the formation of mixed spinel oxides from keeping the TGO structure as a single  $\text{Al}_2\text{O}_3$  layer for a long time.

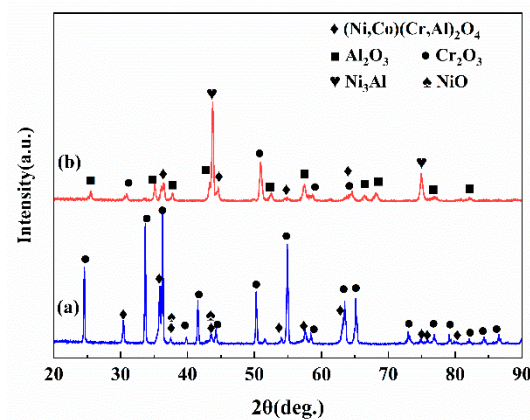


**Figure 11.** XRD pattern of ceramic layer/NiCoCrAlY interface of samples oxidized at 1100 °C for 100 h: (a) AS TBCs and (b) LR TBCs.

#### 4. Conclusions

In this study, AS TBCs and LR TBCs were prepared, and the high-temperature isothermal oxidation and thermally grown oxide (TGO) growth behaviors were studied. The following conclusions can be made:

1. Laser scanning remelting contributed a dense columnar structure to the LZO/YSZ TBCs, and their surface roughness and porosity decreased to 96.3% and 59.1%, respectively, compared to the as-sprayed LZO/YSZ TBCs.
2. Laser scanning remelting presented a crucial inhibition effect on oxygen permeation, and the total TGO growth rate of LR TBCs ( $0.11256 \mu\text{m}^2/\text{h}$ ) was obviously 46.2% lower than that of AS TBCs ( $0.20905 \mu\text{m}^2/\text{h}$ ) during the 1100 °C isothermal oxidation.
3. The  $\text{Al}_2\text{O}_3$  thickness proportion of the total TGO layer in LR TBCs always remained greater than that in the AS TBCs upon the 10 h isothermal oxidization, and laser scanning remelting was effective at inhibiting TGO growth and increasing the high-temperature isothermal oxidation resistance of LZO/YSZ TBCs.

**Author Contributions:** Conceptualization, C.W. and V.V.; methodology, V.V. and J.S.; software, Q.S.; validation, G.A. and Z.L. and G.G.; formal analysis, G.A.; investigation, W.L.; resources, B.C. and Q.S.; data curation, W.L.; writing—original draft preparation, Z.L.; writing—review and editing, G.G.; visualization, J.S.; supervision, W.L.; project administration, W.L.; funding acquisition, W.L. All authors have read and agreed to the published version of the manuscript.

**Funding:** The research was funded by Major Special Projects of Gansu Province [21ZD4WA017], University Industry Transformation Promotion Project of Gansu [2020C-11], and the program of Science and Technology International Cooperation Demonstrative Base of Metal Surface Engineering along the Silk Road [2017D01003] and the “111” project [D21032].

**Institutional Review Board Statement:** Not applicable.

**Informed Consent Statement:** Not applicable.

**Data Availability Statement:** Not applicable.

**Conflicts of Interest:** The authors declare no conflict of interest.

#### References

1. Dhomne, S.; Mahalle, A.M. Thermal barrier coating materials for SI engine. *J. Mater. Res. Technol.* **2018**, *8*, 1532–1537. [[CrossRef](#)]
2. Mehboob, G.; Liu, M.; Xu, T.; Hussain, S.; Mehboob, G.; Tahir, A. A review on failure mechanism of thermal barrier coatings and strategies to extend their lifetime. *Ceram. Int.* **2019**, *46*, 8497–8521. [[CrossRef](#)]

3. Lashmi, P.; Ananthapadmanabhan, P.; Unnikrishnan, G.; Aruna, S. Present status and future prospects of plasma sprayed multilayered thermal barrier coating systems. *J. Eur. Ceram. Soc.* **2020**, *40*, 2731–2745. [[CrossRef](#)]
4. Tailor, S.; Modi, A.; Modi, S. Effect of controlled segmentation on the thermal cycling behavior of plasma sprayed YSZ thick coatings. *Ceram. Int.* **2018**, *44*, 6762–6768. [[CrossRef](#)]
5. Darolia, R. Thermal barrier coatings technology: Critical review, progress update, remaining challenges and prospects. *Int. Mater. Rev.* **2013**, *58*, 315–348. [[CrossRef](#)]
6. Colomban, P.; Jullian, S.; Parlier, M.; Monge-Cadet, P. Identification of the high-temperature impact/friction of aeroengine blades and cases by micro Raman spectroscopy. *Aerosp. Sci. Technol.* **1999**, *3*, 447–459. [[CrossRef](#)]
7. Nath, S.; Manna, I.; Majumdar, J.D. Kinetics and mechanism of isothermal oxidation of compositionally graded yttria stabilized zirconia (YSZ) based thermal barrier coating. *Corros. Sci.* **2014**, *88*, 10–22. [[CrossRef](#)]
8. Cao, X.Q. Development on New Thermal Barrier Coating Materials. *J. Chin. Ceram. Soc.* **2020**, *48*, 1622–1635.
9. Velusamy, R.; Sakthinathan, G.; Vignesh, R.; Kumaraswamy, A.; Sathishkumar, D.; Priya, N.; Krishna, C.S.V. Tribological and thermal characterization of electron beam physical vapor deposited single layer thin film for TBC application. *Surf. Topogr. Metrol. Prop.* **2021**. [[CrossRef](#)]
10. Wu, S.; Zhao, Y.; Li, W.; Liu, W.; Wu, Y.; Liu, F. Research Progresses on Ceramic Materials of Thermal Barrier Coatings on Gas Turbine. *Coatings* **2021**, *11*, 79. [[CrossRef](#)]
11. Higuero, V.; Belzunce, F.J.; Riba, J. High temperature oxidation of plasma and HVOF thermal sprayed CoNiCrAlY coatings in simulated gas turbine and furnace environments. *Surf. Eng.* **2009**, *25*, 319–325. [[CrossRef](#)]
12. Shi, J.; Zhang, T.; Sun, B.; Wang, B.; Zhang, X.; Song, L. Isothermal oxidation and TGO growth behavior of NiCoCrAlY-YSZ thermal barrier coatings on a Ni-based superalloy. *J. Alloys Compd.* **2020**, *844*, 156093. [[CrossRef](#)]
13. An, G.; Li, W.; Feng, L.; Cheng, B.; Wang, Z.; Li, Z.; Zhang, Y. Isothermal oxidation and TGO growth behaviors of YAG/YSZ double-ceramic-layer thermal barrier coatings. *Ceram. Int.* **2021**, *47*, 24320–24330. [[CrossRef](#)]
14. Xie, F.; Sun, Y.; Li, D.; Bai, Y.; Zhang, W. Modelling of catastrophic stress development due to mixed oxide growth in thermal barrier coatings. *Ceram. Int.* **2019**, *45*, 11353–11361. [[CrossRef](#)]
15. Dong, H.; Yang, G.; Li, C.-X.; Luo, X.-T.; Li, C.-J. Effect of TGO Thickness on Thermal Cyclic Lifetime and Failure Mode of Plasma-Sprayed TBCs. *J. Am. Ceram. Soc.* **2014**, *97*, 1226–1232. [[CrossRef](#)]
16. Bai, Y.; Ding, C.H.; Li, H.Q.; Han, Z.H.; Ding, B.J.; Wang, T.J.; Yu, L. Isothermal Oxidation Behavior of Supersonic Atmospheric Plasma-Sprayed Thermal Barrier Coating System. *J. Therm. Spray Technol.* **2013**, *22*, 1201–1209. [[CrossRef](#)]
17. Lakiza, S.M.; Grechanyuk, M.I.; Ruban, O.K.; Redko, V.P.; Glabay, M.S.; Myloserdov, O.B.; Dudnik, O.V.; Prokhorenko, S.V. Thermal Barrier Coatings: Current Status, Search, and Analysis. *Powder Met. Met. Ceram.* **2018**, *57*, 82–113. [[CrossRef](#)]
18. Kumar, V.; Balasubramanian, K. Progress update on failure mechanisms of advanced thermal barrier coatings: A review. *Prog. Org. Coat.* **2016**, *90*, 54–82. [[CrossRef](#)]
19. Liu, B.; Liu, Y.; Zhu, C.; Xiang, H.; Chen, H.; Sun, L.; Gao, Y.; Zhou, Y. Advances on strategies for searching for next generation thermal barrier coating materials. *J. Mater. Sci. Technol.* **2018**, *35*, 833–851. [[CrossRef](#)]
20. Fox, A.; Clyne, T. Oxygen transport by gas permeation through the zirconia layer in plasma sprayed thermal barrier coatings. *Surf. Coat. Technol.* **2004**, *184*, 311–321. [[CrossRef](#)]
21. Cao, X.Q.; Vassen, R.; Tietz, F.; Stoeber, D. New double-ceramic-layer thermal barrier coatings based on zirconia–rare earth composite oxides. *J. Eur. Ceram. Soc.* **2006**, *26*, 247–251. [[CrossRef](#)]
22. Zhang, J.; Guo, X.; Jung, Y.-G.; Li, L.; Knapp, J. Lanthanum zirconate based thermal barrier coatings: A review. *Surf. Coat. Technol.* **2017**, *323*, 18–29. [[CrossRef](#)]
23. Liu, X.Y.; Che, J.W.; Yi, H.; Zhang, J.; Liang, G.Y. Diffusion mechanism of oxygen ions in La<sub>2</sub>Zr<sub>2</sub>O<sub>7</sub>/YSZ composite ceramics. *J. Alloys Compd.* **2018**, *778*, 522–531. [[CrossRef](#)]
24. Wang, Y.; Wang, L.; Liu, S.Y. Thermal spraying of nanostructured La<sub>2</sub>Zr<sub>2</sub>O<sub>7</sub>(LZ)/8YSZ dual ceramic thermal barrier coatings. *China Surf. Eng.* **2016**, *29*, 16–24. (In Chinese)
25. Xu, Z.; He, L.; Mu, R.; Zhong, X.; Zhang, Y.; Zhang, J.; Cao, X. Double-ceramic-layer thermal barrier coatings of La<sub>2</sub>Zr<sub>2</sub>O<sub>7</sub>/YSZ deposited by electron beam-physical vapor deposition. *J. Alloys Compd.* **2009**, *473*, 509–515. [[CrossRef](#)]
26. Zaplatynsky, I. Performance of laser-glazed zirconia thermal barrier coatings in cyclic oxidation and corrosion burner rig tests. *Thin Solid Films* **1982**, *95*, 275–284. [[CrossRef](#)]
27. Ahmaniemi, S.; Tuominen, J.; Vippola, M.; Vuoristo, P.; Mäntylä, T.; Cernuschi, F.; Gualco, C.; Bonadei, A.; Di Maggio, R. Characterization of Modified Thick Thermal Barrier Coatings. *J. Therm. Spray Technol.* **2004**, *13*, 361–369. [[CrossRef](#)]
28. Xu, S.Q.; Zhu, C.; Zhang, Y. Effects of Laser Remelting and Oxidation on NiCrAlY/8Y<sub>2</sub>O<sub>3</sub>-ZrO<sub>2</sub> Thermal Barrier Coatings. *J. Therm. Spray Technol.* **2017**, *27*, 412–422. [[CrossRef](#)]
29. Antou, G.; Montavon, G.; Hlawka, F.; Cornet, A.; Coddet, C.; Machi, F. Modification of ceramic thermal spray deposit microstructures implementing in situ laser remelting. *Surf. Coat. Technol.* **2003**, *172*, 279–290. [[CrossRef](#)]
30. Batista, C.; Portinha, A.; Ribeiro, R.; Teixeira, V.; de Oliveira, C.A.R. Evaluation of laser-glazed plasma-sprayed thermal barrier coatings under high temperature exposure to molten salts. *Surf. Coat. Technol.* **2006**, *200*, 6783–6791. [[CrossRef](#)]
31. Balla, V.K.; Bandyopadhyay, P.P.; Bose, S.; Bandyopadhyay, A. Compositionally graded yttria-stabilized zirconia coating on stainless steel using laser engineered net shaping (LENS<sup>TM</sup>). *Scr. Mater.* **2007**, *57*, 861–864. [[CrossRef](#)]

32. Ahmadi-Pidani, R.; Shoja-Razavi, R.; Mozafarinia, R.; Jamali, H. Improving the thermal shock resistance of plasma sprayed CYSZ thermal barrier coatings by laser surface modification. *Opt. Lasers Eng.* **2012**, *50*, 780–786. [[CrossRef](#)]
33. de Freitas, F.E.; Briguente, F.P.; dos Reis, A.G.; de Vasconcelos, G.; Reis, D.A.P. Investigation on the microstructure and creep behavior of laser remelted thermal barrier coating. *Surf. Coat. Technol.* **2019**, *369*, 257–264. [[CrossRef](#)]
34. Zhao, C.; Zhao, M.; Shahid, M.; Wang, M.; Pan, W. Restrained TGO growth in YSZ/NiCrAlY thermal barrier coatings by modified laser remelting. *Surf. Coat. Technol.* **2017**, *309*, 1119–1125. [[CrossRef](#)]
35. Guo, L.; Xin, H.; Zhang, Z.; Zhang, X.; Ye, F. Microstructure modification of Y<sub>2</sub>O<sub>3</sub> stabilized ZrO<sub>2</sub> thermal barrier coatings by laser glazing and the effects on the hot corrosion resistance. *J. Adv. Ceram.* **2020**, *9*, 232–242. [[CrossRef](#)]
36. Izadinia, M.; Soltani, R.; Sohi, M.H. Effect of segmented cracks on TGO growth and life of thick thermal barrier coating under isothermal oxidation conditions. *Ceram. Int.* **2019**, *46*, 7475–7481. [[CrossRef](#)]
37. Morks, M.; Berndt, C.; Durandet, Y.; Brandt, M.; Wang, J. Microscopic observation of laser glazed yttria-stabilized zirconia coatings. *Appl. Surf. Sci.* **2010**, *256*, 6213–6218. [[CrossRef](#)]
38. Chen, H.F.; Liu, Y.; Gao, Y.F.; Luo, H.J.; Tao, S.Y.; Luo, H.J. Design, Preparation, and Characterization of Graded YSZ/La<sub>2</sub>Zr<sub>2</sub>O<sub>7</sub> Thermal Barrier Coatings. *J. Am. Ceram. Soc.* **2010**, *93*, 1732–1740.
39. Cheng, B.; Yang, G.-J.; Zhang, Q.; Yang, N.; Zhang, M.; Zhang, Y.; Li, C.-X.; Li, C.-J. Gradient thermal cyclic behaviour of La<sub>2</sub>Zr<sub>2</sub>O<sub>7</sub>/YSZ DCL-TBCs with equivalent thermal insulation performance. *J. Eur. Ceram. Soc.* **2017**, *38*, 1888–1896. [[CrossRef](#)]
40. Feng, Y.; Dong, T.-S.; Li, G.-L.; Wang, R.; Zhao, X.-W.; Liu, Q. High temperature oxidation resistance and TGO growth mechanism of laser remelted thermal barrier coatings. *J. Alloys Compd.* **2020**, *828*, 154266. [[CrossRef](#)]
41. Hu, Y.; Cai, C.; Wang, Y.; Yu, H.; Zhou, Y.; Zhou, G. YSZ/NiCrAlY interface oxidation of APS thermal barrier coatings. *Corros. Sci.* **2018**, *142*, 22–30. [[CrossRef](#)]
42. Ullah, A.; Khan, A.; Bao, Z.; Yu, C.; Zhu, S.; Wang, F. Effect of vacuum annealing on initial oxidation behavior and alumina transition of NiCoCrAlY coatings. *Surf. Coat. Technol.* **2020**, *404*, 126441. [[CrossRef](#)]
43. Zhou, S.; Xiong, Z.; Lei, J.; Dai, X.; Zhang, T.; Wang, C. Influence of milling time on the microstructure evolution and oxidation behavior of NiCrAlY coatings by laser induction hybrid cladding. *Corros. Sci.* **2016**, *103*, 105–116. [[CrossRef](#)]
44. Doleker, K.M.; Ozgurluk, Y.; Karaoglanli, A.C. Isothermal oxidation and thermal cyclic behaviors of YSZ and double-layered YSZ/La<sub>2</sub>Zr<sub>2</sub>O<sub>7</sub> thermal barrier coatings (TBCs). *Surf. Coatings Technol.* **2018**, *351*, 78–88. [[CrossRef](#)]
45. Zheng, L.; Zhang, M.C.; Chellali, R.; Bouchikhaoui, H.; Dong, J.X. Oxidation property of powder metallurgy EP741NP Ni based superalloy at elevated temperatures. *Mater. Technol.* **2013**, *28*, 122–128. [[CrossRef](#)]
46. Dong, T.-S.; Wang, R.; Di, Y.-L.; Wang, H.-D.; Li, G.-L.; Fu, B.-G. Mechanism of high temperature oxidation resistance improvement of double-layer thermal barrier coatings (TBCs) by La. *Ceram. Int.* **2019**, *45*, 9126–9135. [[CrossRef](#)]
47. Zhang, P.; Zhang, X.; Li, F.; Zhang, Z.; Wang, Y.; Li, H.; Ren, L.; Liu, M. Hot Corrosion Behavior of YSZ Thermal Barrier Coatings Modified by Laser Remelting and Al Deposition. *J. Therm. Spray Technol.* **2019**, *28*, 1225–1238. [[CrossRef](#)]
48. Sun, H.-Y.; He, Q.; Zhou, Z.-J.; Wang, M.; Zhang, G.-M.; Li, S.-F. Effects of solution depletion and segregation oxidation on morphology of modified 310 austenitic stainless steel. *J. Iron Steel Res. Int.* **2016**, *23*, 393–400. [[CrossRef](#)]